Structural, magnetic, and transport properties of substitutionally doped graphene nanoribbons from first principles

E. Cruz-Silva, Z. M. Barnett, B. G. Sumpter, and V. Meunier

Phys. Rev. B **83**, 155445 — Published 26 April 2011

DOI: 10.1103/PhysRevB.83.155445

Structural, magnetic, and transport properties of substitutionally doped graphene nanoribbons from first-principles

E. Cruz-Silva[1], Z. M. Barnett[2], B.G. Sumpter[1], and V. Meunier[1, 3].

[1] Oak Ridge National Laboratory, P.O. Box 2008, Oak Ridge, TN 37831-6367, USA

[2] Department of Physics and Astronomy, University of Tennessee, Knoxville, TN 37996, USA

[3] Department of Physics, Applied Physics, and Astronomy, Rensselaer Polytechnic Institute, Troy, NY 12180-3590, USA

Abstract

We present a study of the electronic properties of narrow zigzag and armchair nanoribbons substitutionally doped with a single boron, nitrogen, or phosphorus atom. Using density functional calculations, we analyze the formation energy, electronic band structure, magnetic, and quantum conductance properties of these nanoribbons with doping sites ranging from the edge to the center of the ribbon. Substitutional doping is found to be most favorable at the ribbon edge in all the cases except for the boron-doped armchair ribbon, which has the lowest formation energy in the three-coordinated site next to the edge. Boron-doped zigzag nanoribbons exhibit spin-dependent donor-like states when the dopant is on the ribbon edge, and acceptor states as the dopant is moved toward the ribbon center. Nitrogen doped zigzag nanoribbons show the opposite effect, while phosphorus doped nanoribbons exhibit both donor-like and acceptor-like states. The band structure and local density of states indicate that dips in conductance occur from either the presence of a localized state or the opening of mini band-gaps around a particular energy value. The variations in conductance arising from different doping profiles could be useful for tailoring the properties of graphene-based nanoelectronic devices

1. Introduction

In recent years, the research and understanding of electron transport within graphene and graphitic nanoribbons (GNRs) has increased greatly due to the promise of their tunable properties, which can lead to future technologically advanced electromagnetic devices that are low-cost and easy to manufacture[1]. Graphitic nanoribbons have rapidly become a focus of study both as a relatively simple test system for carbon nanotube investigation[2] and for their own unique properties, which stem for instance from the edge states associated to sharp edges in GNRs[1,3]. Among the potential uses of GNRs, recent studies have investigated the magnetic properties of zigzag-edge nanoribbons (zGNRs) and the possibility of controlling their conductance leading to spin-polarised conductors[4-6]. Other studies have been focused on the study of dopant-dependent conductance of GNRs as a means of constructing sensors for gas molecules.[7] Additional investigations have highlighted the properties of heterojunctions between armchair and zigzag GNRs seamed together with a row of pentagon-heptagon pairs, while keeping the threefold coordination of each atom.[8] In spite of the already extensive understanding of GNR's properties and because of the promise these structures hold for the design of novel nanoscale devices and interconnects, considerable research is still necessary to fully understand their electrical properties and thermal stability before that promise can be fully realized.

While the doping of carbon nanotubes has been extensively studied as a means of controlling nanotube growth[9,10] as well as tuning the electronic properties of both single-wall carbon nanotubes[2,11] and double-wall nanotubes[12], there has been less research to date on the effect of doping on graphene nanoribbons. Practical doping of graphene has been devised by several methods, which include electrothermal reactions of graphene[13], hydrocarbon pyrolysis in presence of ammonia[14], and arc discharge[15], among others. The effect of boron and nitrogen doping on zigzag nanoribbons on the order of 1 nm has been reported by Martins *et al.*[16,17] These works were recently complemented by the works of Biel *et al.*[18] and Zheng *et al.* [19], with studies revealing unusual acceptor-donor effects of both boron-doped and nitrogen-doped nanoribbons. Further studies of the electronic properties of graphene nanoribbons have shown that these can exhibit half-metallic behavior, either by applying transverse electric fields[20] or by suppressing one of the edge states[8].

In this paper, we present a systematic study of the spin polarized electronic and transport

properties of zigzag and armchair nanoribbons substitutionally doped with boron, nitrogen, and phosphorus. The goal of this work is to improve the existing understanding of the structural properties and spin-dependent electronic behavior of boron, nitrogen, and phosphorus doping in both zigzag and armchair nanoribbons.

2. Methods

Two different systems were considered to investigate the effects of substitutional doping on graphene nanoribbons: a 12-zGNR (zigzag graphene nanoribbon) with a width of 1.13 nm and a length of 2.83 nm, and an 11-aGNR (armchair graphene nanoribbon) with a width of 1.39 nm and a length of 1.2 nm. Here, the numbers preceding the nanoribbon type refer to the number of carbon atoms along the width of the ribbon. A unit cell of each ribbon type is shown in **Fig 1**. Twelve such unit cells were considered for the 12-zGNR systems and five for the 11-aGNR systems, with a dopant atom in only one unit cell. The edges of both ribbons were fully passivated with hydrogen atoms to increase thermodynamic stability[3], and a minimum lateral distance of 10 Å was maintained between supercells in the GNR's finite-size dimensions. We determined that a real-space mesh equivalent to a plane-wave cutoff energy of 200 Ry for real-space integrals was sufficient to achieve convergence in the total energy within 1 meV. The Brillouin zone was sampled using a Monkhorst-Pack grid corresponding to 8 k-points in the ribbon growth direction.[21] LDA functionals using the Ceperley-Alder implementation were used for all the calculations.[22] We employed a basis-set made up of double-ξ with single polarization orbitals, with an energy shift of 0.2721 eV[23]. The coordinates of all systems were relaxed by conjugate gradient minimization until the maximum force was less than 0.04 eV/Å.

Doping was achieved by substituting a single carbon atom with a nitrogen, boron, or phosphorus atom. The atomic dopant was initially displaced slightly above the plane of the ribbon (~ 0.2 Å) in order to avoid trapping the structure in a high symmetry, metastable position. *Ab initio* calculations to obtain the final relaxed structure, band structure, and charge density calculations of each system were performed using SIESTA with parameters outlined above[24]. Conductance and density of states calculations were performed using our in-house transport code based on the Landauer-Büttiker formalism outlined by Datta[25] and used in previous similar studies[8,26-28]. The converged Hamiltonian from the SIESTA calculation was used as starting point for the conductance studies. It has been previously shown that the spin alignment of the localized edge

states on zigzag nanoribbons can have either ferromagnetic or antiferromagnetic alignment, and that the magnetic interaction strength decreases with the nanoribbon width. Therefore, all zigzag nanoribbons are studied in their anti-ferromagnetic configuration, as it was found to be the most energetically stable.[1]

We also note that band structure calculations do not correlate exactly with the calculations for the conductance and the density of states as the conductance and density of states calculations were performed using a doped, finite system connected to semi-infinite pristine graphene leads (a so- called "open-system"), whereas the band structure calculations performed in SIESTA assumed a doped, periodic superlattice. This difference in boundary conditions can introduce a number of notable effects, including variations in level broadening, energy gaps, and energy shifts. The latter effect can be accounted for by shifting the Fermi energy to the zero energy value. Note that in the transport calculations, care must be taken when calculations for electrodes and conductor are done separately. While it is straightforward to connect the two calculations to assemble the open systems, it is also important to align the Fermi level of the leads with that of the scattering region to avoid building up an artificial Shottky barrier at the lead-conductor interface.[29]

3. Results and Discussion

The results of our calculations (**Fig. 1**) indicate that for doped 12-zGNR systems, the most stable dopant position, corresponding to the lowest energy configuration, occurs when the dopant is located at the edge of the ribbon (site #1, **Fig. 1**). While this result is consistent for N, B, and P, the situation is notably different in the case of the armchair GNR. The lowest energy configurations for nitrogen and phosphorus doping occurs when the dopant is at the ribbon edge, but the lowest energy is found at site #2 for the boron-doped system. Note that for B-doped and N-doped 11-aGNRs, the relative formation energy graph is quite flat (**Fig. 1**), showing that metastable positions are not ruled out for practical thermodynamical conditions. Here the relative formation energy was computed using the following equation:

$$E_R = E_N - E_{GS} \qquad (1)$$

where E_R is the relative formation energy of the doped structure, E_N is the total energy for the

GNR with the doping atom in site N, and E_{GS} is the total energy of the doped structure ground state. First-principles calculations have previously indicated that quantum size effects strongly affect the incorporation of defect atoms into nanocrystals, showing that substitutional positions near the surface are more stable, for instance in the case of B and P in silicon[30], or Mn in CdSe and ZnSe nanocrystals[31]. In **Table I**, we present a detailed list of the bond lengths and bond angles for the dopant atom and its nearest neighbors for the most energetically favorable structures. The table also includes two cases of P-doped 11-aGNR structures (site #3 and site #6) since they display unusual spin-dependent behavior and magnetization. In each column, X represents the dopant atom. Y_1, Y_2, and Y_3 represent the nearest neighbor atoms, i.e. either C or H depending on the system. Below we discuss the electronic properties for each case in detail.

3.1 Boron-doped ribbons

Our findings are consistent with those of Biel *et al.*[18] who used non-spin polarized calculations to show that doping zigzag nanoribbons with B induces the expected acceptor-like states (i.e., below the Fermi level) when placed at the center of the ribbon, as well as more unusual donor-like states (i.e., above the Fermi level) when placed at the ribbon's edge. Note that our spin-dependent calculations show different energy level positions for spin up and spin down electronic states (**Fig. 2a**), in agreement with the results of Zheng *et al.*[19], and Martins et al.[17], thereby suggesting the possibility of using such ribbons as spin valves.

Unlike carbon, boron has only three electrons in its valence shell, and when present in sp^2 bonded carbon the missing p_z electrons behave as "holes" in the carbon π orbital network. These holes are partially filled by the delocalized electrons in the π network, and hence boron behaves as an electron acceptor. It follows that the calculated donor-like state for boron doped nanoribbons is quite unexpected. The density of states reveals that the drops in spin up and spin down conductance above the Fermi energy are due to the presence of a localized state in those energy ranges. A comparison with the band structure further corroborates this conclusion, as a localized state (flat band) for spin up and spin down electrons is observed in the corresponding energy range. The charge density plot of the system further confirms the presence of localized states and places them at the site of the dopant (**Figs. 2b and 2c**). As the boron-centered acceptor is moved closer to the nanoribbon zigzag edge states, electrostatic repulsion effects

increase the energy of the acceptor state, shifting it towards higher energies, as observed in the density of states plot (**Fig. 3**), until reaching the conductance band, where a behavior akin to a donor-like system is observed. Of course, the boron atom does not become a donor but the density of states show localized states reminiscent of a donor-states. This effect simply means that the perturbation brought about by the chemical doping cannot be treated as a mere first-order perturbation since strong electrostatic repulsion is induced when the dopant is close to the system's edge.

The B-doped ribbons also exhibit a partial drop in spin up conductance, compared to that of the pristine system, just below the Fermi energy. A reduced density of spin up states appears in this energy range, which is caused by a mini-gap opening in the band structure for spin up states that partially covers this range. Charge density plots further confirm this behavior, showing a localized depletion of states at the dopant site (**Fig. 2d**).

Turning to boron-doped armchair nanoribbons, these systems display the expected acceptor state for all dopant configurations. However, in the case of boron doping, the most energetically favorable dopant configuration for armchair nanoribbons is site #2 instead of site #1. Our calculations reveal no spin-dependence in this and all other doped armchair structures, with the exception of the P-doped (site #3) and P-doped (site #6) of 11-aGNRs (see section 3.3). As with the zigzag-doped nanoribbon, we observe an increase in the density of states and a flat band in the energy range of the conductance dip (**Fig. 4a**), indicating the presence of a localized state, as corroborated by the charge density plots (**Fig. 4b**). Note that the absence of donor-like states when boron is close to the edge can be explained by the reduced electrostatic repulsion at the edge, since, unlike the zigzag case, there is no 1D state localized along the edge of armchair systems around the Fermi level.

3.2. N-doped ribbons

N-doped zigzag ribbons show the expected donor state when N is placed at the center of the ribbon and, similar to boron, show an opposite acceptor-like state when N is placed at the edge of the ribbon. As the configuration with N placed at the edge of the ribbon was the most energetically favorable, we focused our attention to this configuration. Spin-polarized calculations show another case of clear spin-dependent transport behavior (**Fig. 5a**).

Both drops in conductance below the Fermi energy correspond to increases in the density of states and a pair of flattened bands, showing another localized state as seen in the charge density calculations (**Figs. 5b, 5c**). A partial drop in spin up conductance also occurs in this system. This reduction appears to be caused by another mini-gap opening in the band structure, producing the depletion of states seen in the charge density calculation (**Fig. 5d**).

The N-doped armchair ribbons display spin-degenerate behavior, just as in the case of the B-doped armchair ribbons. The expected donor-like state is seen in the conductance plot when the dopant is on the ribbon edge (**Fig. 6**). An increased density of states appears in this energy range, in correlation with the flattened band found in the same energy range.

When doping graphitic materials, the fifth electron that nitrogen possesses in its valence shell spills into the π^* band in the sp^2 carbon network. It follows that an electron donor behavior is usually observed. As the nitrogen position is moved towards the zigzag edge, the localized donor experiences an electrostatic attraction by the nanoribbon's edge state, and its energy is shifted towards the valence bands where it behaves as an electron acceptor, as shown in **figure 7**. Again, the absence of edge states in the armchair ribbons explains that such acceptor-like behavior is absent in that case.

3.3 P-doped ribbons

When the phosphorus dopant is placed on the edge of the zigzag ribbon, a significant structural distortion in the ribbon is introduced due to the sp^3 character and length of the P-C atomic bond, as previously discussed.[2] This effect causes the H atom bonded to the P dopant to be rotated out-of the plane of the ribbon. The dopant induces both a donor state and an acceptor state (**Fig. 8a**). Density of states and band structure calculations reveal that both cases are caused by the presence of localized electronic states. The P-doped zigzag ribbons also display the same drop in spin-up conductance just below the Fermi energy, as we also observed in the B-doped and N-doped zigzag ribbons.

In armchair ribbons, P-doping in site #1 leads to a rather wide drop in conductance centered around the Fermi energy due to the presence of a localized state in the energy range surrounded

by band gaps (**Fig 8b**). Furthermore, when the dopant is placed in sites #3 or #6, a large magnetization appears due to a significant deviation from the normally spin independent behavior of the doped armchair ribbons. This spin dependent behavior appears as a large spike in the density of states for spin-down electrons above the Fermi energy, as well as a smaller spike in the density of states for spin-up electrons just above the Fermi energy (**Fig 9**). Both spikes are due to flattened bands in the corresponding energy range. Charge density calculations confirm the presence of a highly spatially localized state at the site of the phosphorus atom in both structures (**Fig 10**). When the dopant is at site #3, this localized state manifests as a narrow drop in the conductance. However, we do not observe a similar effect on the conductance when the dopant is in site #6. In the case of the dopant in site #6, these localized states occur in the center of the ribbon, without perturbing the symmetry of the system, and hence preventing them from interfering with the conductance channels.

Finally, we turn to the magnetic properties of doped nanoribbons. It is interesting to notice that doped zigzag nanoribbons have a net magnetic moment that increases as the dopant position is moved towards the edge of the ribbon; while all armchair nanoribbons have a null magnetic moment. In previous studies, it has already been found that boron or nitrogen doping of other graphitic paramagnetic structures, such as carbon nanotubes or two dimensional graphene, results also in a paramagnetic behavior[2]. It was also found that the high localization of the bound state in phosphorus leads to a splitting of this state and the appearance of a net magnetic moment,[11] in agreement with other studies of localized defects on graphene[32]. In this study, it is found that only P-doped armchair nanoribbons with the P atom on sites #3 and #6 have a magnetic moment close to $0.9\mu_B$, and show a strong splitting of the quasibound state of ca. 0.25 eV. In the case of boron and nitrogen doped zigzag nanoribbons, the total magnetic moment increases from less than $0.1\mu B$ to $1\mu B$ as the atom position moves towards the edge of the ribbon, probably due to the interplay between the nanoribbons edge state and the dopant semilocalized states, which also affects the energy of the later, as shown in figs. 3 and 7. It is followed that the different spins of the localized state experience a different interaction with the edge state, which results in a splitting of the former. A similar trend is observed for the phosphorus doped zGNRs, with the exception of position #5, where the localization of the state causes splitting and a net moment of $1\mu_B$.

Conclusions

In summary, we have determined the most energetically favorable configurations of boron-doped, nitrogen-doped, and phosphorus-doped zigzag and armchair nanoribbons and have highlighted interesting spin-dependent behaviors. Nitrogen and phosphorus atoms preferentially substitute at the edges of zigzag and armchair nanoribbons, whereas boron atoms preferentially substitute at the edges of zigzag nanoribbons but next to the edge of armchair nanoribbons. Spin-dependent conductance was found in the most energetically favorable boron-doped and nitrogen-doped zigzag nanoribbons, leading to the possibility of utilizing such structures in spintronic devices. The most favorable configuration of phosphorus atoms did not present a significant degree of spin-dependent behavior, but it did display both a donor-like and an acceptor-like state. Doped armchair nanoribbon conductance behavior was spin-degenerate for all cases, but in phosphorus-doped armchair ribbons, spin-dependent behavior emerged in the density of states and band structure when the dopant was placed in sites #3 or #6.

Acknowledgements: The authors acknowledge support from the Laboratory Directed Research and Development Program of ORNL and from U.S. Department of Energy under Contract No. DEAC05-00OR22725 with UT-Battelle, LLC at ORNL. Part of this work was supported by the Center for Nanophase Materials Sciences (CNMS), sponsored by the Division of Scientific User Facilities, U.S. Department of Energy and by the Division of Materials Science and Engineering, Basic Energy Sciences, U.S. Department of Energy. Calculations were done using the resources of ORNL Institutional Clusters (OIC) and the National Center for Computational Sciences (NCCS).

References

1. L. Pisani, J.A. Chan, B. Montanari, and N.M. Harrison, Phys. Rev. B **75**, 064418 (2007).
2. E. Cruz-Silva, F. Lopez-Urias, E. Munoz-Sandoval, B.G. Sumpter, H. Terrones, J.-C. Charlier, V. Meunier, and M. Terrones, ACS Nano **3**, 1913 (2009).
3. V. Barone, O. Hod, and G.E. Scuseria, Nano Lett. **6**, 2748 (2006).
4. O.V. Yazyev, Rep. Prog. Phys. **73**, 056501 (2010).
5. O.V. Yazyev and M.I. Katnelson, Phys. Rev. Lett. **100**, 047209 (2008)
6. G. Cantele, Y.-S. Lee, D. Ninno, and N. Marzari, Nano Letters, **9** 3425 (2009).
7. Y. Zhang, Y. Chen, K. Zhou, C. Liu, J. Zeng, H. Zhang, and Y. Peng, Nanotechnology **20**, 185504 (2009).
8. A.R. Botello-Méndez, E. Cruz-Silva, F. López-Urías, B.G. Sumpter, V. Meunier, M. Terrones, and H. Terrones, ACS Nano **3**, 3606 (2009).
9. B.G. Sumpter, V. Meunier, J.M. Romo-Herrera, E. Cruz-Silva, D.A. Cullen, H. Terrones, D.J. Smith, and M. Terrones, ACS Nano **1**, 369 (2007).
10. J.M. Romo-Herrera, B.G. Sumpter, D.A. Cullen, H. Terrones, E. Cruz-Silva, D.J. Smith, V. Meunier, and M. Terrones, Angew. Chem. Int. Edit. **47**, 2948 (2008).
11. I.O. Maciel, J. Campos-Delgado, E. Cruz-Silva, M.A. Pimenta, B.G. Sumpter, V. Meunier, F. Lopez-Urias, E. Munoz-Sandoval, H. Terrones, M. Terrones, and A. Jorio, Nano Lett. **9**, 2267 (2009).
12. A.G. Souza Filho, V. Meunier, M. Terrones, B.G. Sumpter, E.B. Barros, F. Villalpando-Páez, J. Mendes Filho, Y.A. Kim, H. Muramatsu, T. Hayashi, M. Endo, and M.S. Dresselhaus, Nano Lett. **7**, 2383 (2007).
13. X. Wang, X. Li, L. Zhang, Y. Yoon, P.K. Weber, H. Wang, J. Guo, and H. Dai, Science **324**, 768 (2009).
14. L. Qu, Y. Liu, J. Baek, and L. Dai, ACS Nano **4**, 1321-1326 (2010).
15. K.S. Subrahmanyam, L.S. Panchakarla, A. Govindaraj, and C.N.R. Rao, J. Phys. Chem. C **113**, 4257 (2009).
16. T.B. Martins, R.H. Miwa, A.J.R. da Silva, and A. Fazzio, Phys. Rev. Lett. **98**, 196803 (2007).
17. T.B. Martins, A.J.R. da Silva, R.H. Miwa, and A. Fazzio, Nano Lett. **8**, 2293 (2008).
18. B. Biel, X. Blase, F. Triozon, and S. Roche, Phys. Rev. Lett. **102**, 096803 (2009).
19. X. H. Zheng, I. Rungger, Z. Zeng and S. Sanvito, Phys. Rev. B **80**, 235426 (2008).

20. Y.-W. Son, M.L. Cohen, and S.G. Louie, Nature **444**, 347 (2006).
21. H. Monkhorst and J. Pack, Phys. Rev. B **13**, 5188 (1976).
22. D. Ceperley and B. Alder, Phys. Rev. Lett. **45**, 566 (1980).
23. J. Junquera, O. Paz, D. Sánchez-Portal, and E. Artacho, Phys. Rev. B **64**, 23511 (2001).
24. J.M. Soler, E. Artacho, J.D. Gale, A. Garcia, J. Junquera, P. Ordejon, and D. Sanchez-Portal, J. Phys.: Condens. Matter **14**, 2745 (2002).
25. S. Datta, *Quantum Transport : Atom to Transistor* (Cambridge University Press, Cambridge UK, 2005).
26. V. Meunier and B.G. Sumpter, J. Chem. Phys. **123**, 024705 (2005).
27. V. Meunier, M. Buongiorno Nardelli, C. Roland, and J. Bernholc, Phys. Rev. B **64**, 195419 (2001).
28. J.M. Romo-Herrera, M. Terrones, H. Terrones, and V. Meunier, Nanotechnology **19**, 315704 (2008).
29. V. Meunier, M.B. Nardelli, J. Bernholc, T. Zacharia, and J.-C. Charlier, Appl. Phys. Lett. **81**, 5234 (2002).
30. G. Cantele, E. Degoli, E. Luppi, R. Magri, D. Ninno, G. Iadonisi, and S. Ossicini, Phys. Rev. B **72**, 113303 (2005).
31. T.-L. Chan, A.T. Zayak, G.M. Dalpian, and J.R. Chelikowsky, Phys. Rev. Lett. **102**, 025901 (2009).
32. O.V. Yazyev and L. Helm, Phys. Rev. B **75**, 125408 (2007).

Figures and tables:

Table I. The computed bond lengths between the dopant atom and each of its nearest neighbors and the angle formed by each pair of nearest neighbors and the dopant atom. In each structure, X represents the dopant atom, whereas the atoms represented by Y_1, Y_2, and Y_3 are noted in each row.

Structure and Dopant Site	Y_1	Y_2	Y_3	X-Y_1 Bond Length [Å]	X-Y_2 Bond Length [Å]	X-Y_3 Bond Length [Å]	Y_1-Y_2 Bond Angle [deg]	Y_2-Y_3 Bond Angle [deg]	Y_1-Y_3 Bond Angle [deg]
12-zGNR (B1)	H	C	C	1.23	1.51	1.51	121.60	116.56	121.84
12-zGNR (N1)	H	C	C	1.02	1.38	1.38	117.31	125.67	117.03
12-zGNR (P1)	H	C	C	1.47	1.79	1.79	95.27	98.91	94.89
11-aGNR (B2)	C	C	C	1.50	1.51	1.51	118.81	116.91	124.27
11-aGNR (N1)	H	C	C	1.02	1.35	1.36	118.90	124.34	116.76
11-aGNR (P1)	H	C	C	1.47	1.73	1.79	100.30	99.66	101.57
11-aGNR (P3)	C	C	C	1.76	1.75	1.75	103.08	101.68	102.65
11-aGNR (P6)	C	C	C	1.75	1.75	1.75	101.51	101.86	101.85

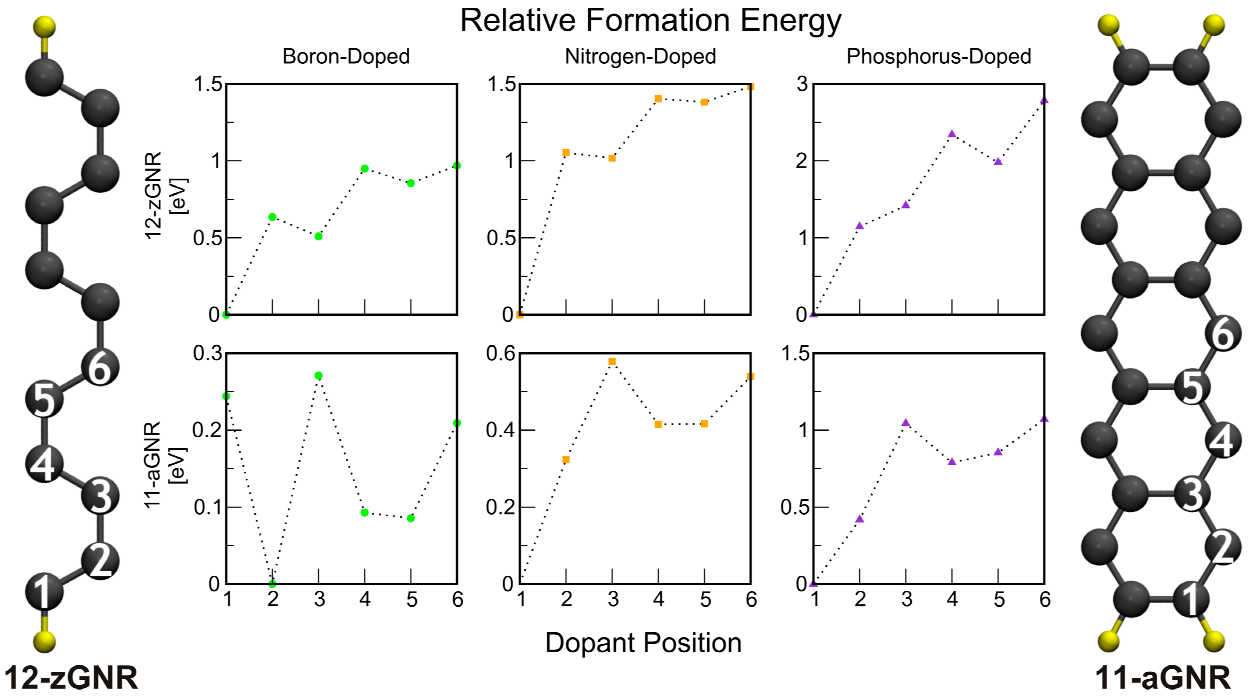

Figure 1: (color online) Relative formation energy for each dopant position in the zigzag and armchair nanoribbons. The horizontal axis corresponds to the dopant's position along the width of the ribbon, moving inward from site #1 (ribbon edge) to site #6 (ribbon center), as shown on the ball-and-sticks models.

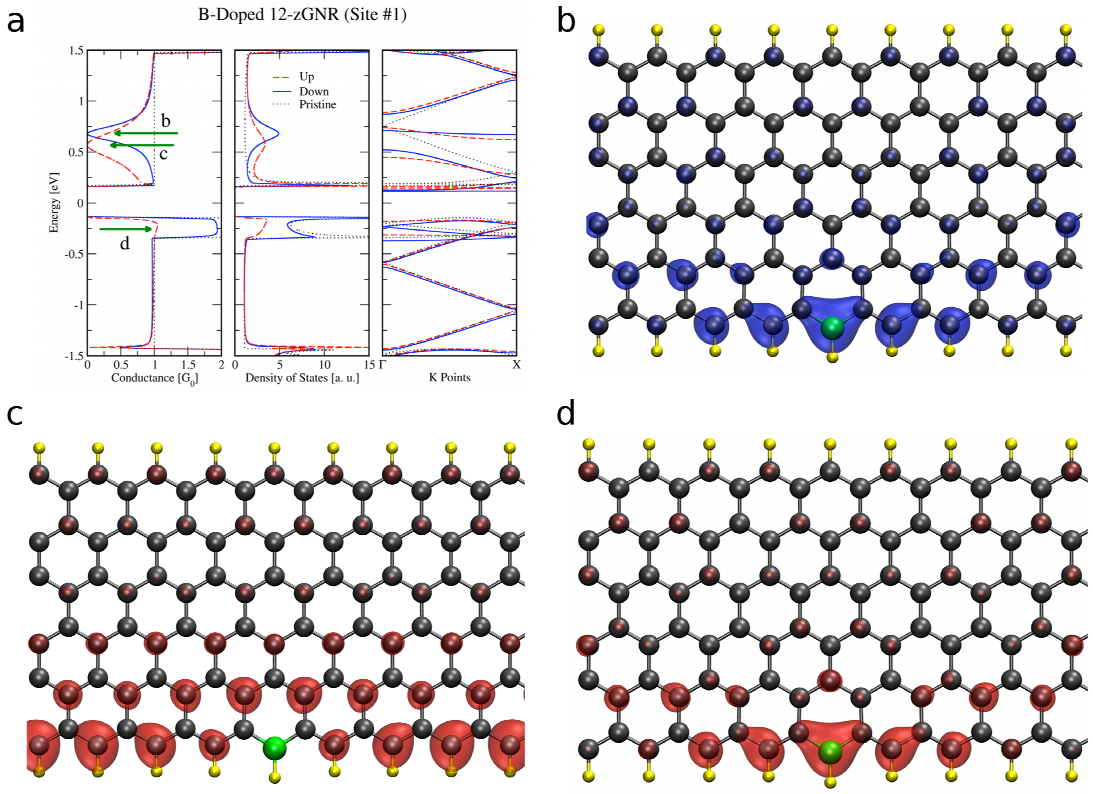

Figure 2: (color online) (a) Conductance and density of states, for the B-doped (site #1) 12-zGNR structure connected to semi-infinite electrodes (open system), and band structure for a periodic B-doped (site #1) 12-zGNR structure (periodic system) where spin-dependent behavior is observed. Energies are relative to the Fermi energy of the leads. The arrows mark the approximate energy ranges of the charge density calculations in b, c, and d. (b) Spin down charge density for the energy range 0.48 eV to 0.72 eV. (c) Spin up charge density for the energy range 0.62 eV to 0.82 eV. (d) Spin up charge density for the energy range -0.31 eV to -0.11 eV. All isosurfaces are drawn at density=0.005 e·Bohr^{-3}, H atoms are shown in light color (yellow), C atoms are shown in gray, and B atoms are shown as lighter gray (green) circles.

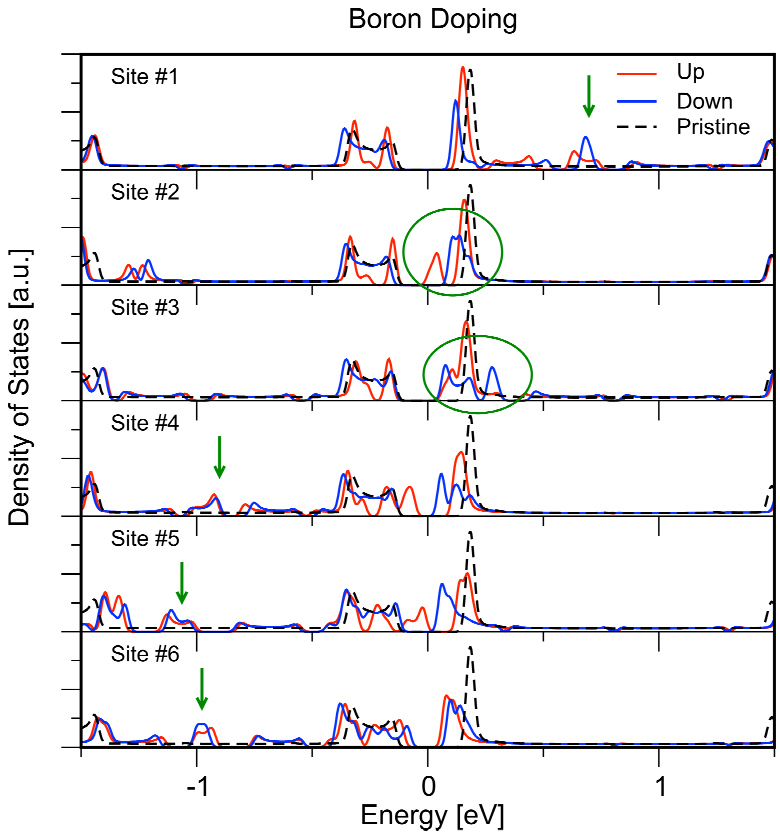

Figure 3: (color online) Density of states for boron-doped zigzag graphene nanoribbons, where the doping atom position is moved from the central position (site #6, bottom) to the edge of the nanoribbons (site #1, top). As the atom is moved closer to the edge, electrostatic interactions between the localized states and the carbon edge state cause shifts in the energy of the localized states (arrows, sites #4-6), splitting of the edge states (circled areas, sites #2-3) and finally the shift of the localized state towards the conduction bands (arrow, site #1). Energies are relative to the pristine nanoribbon's Fermi energy.

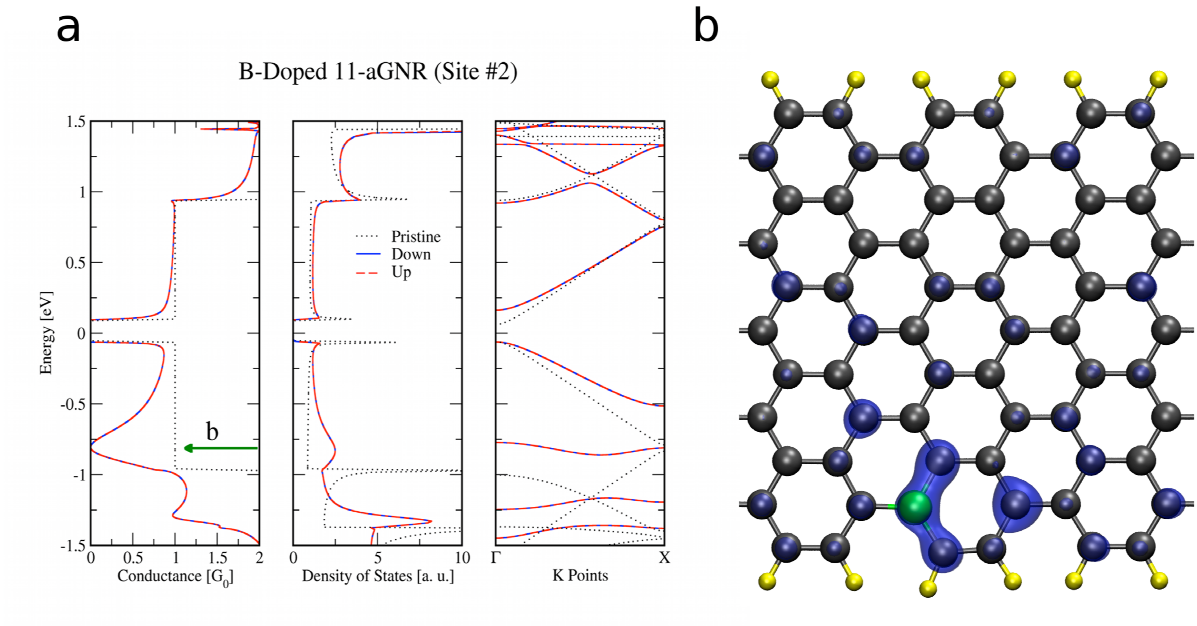

Figure 4: (color online) (a) Conductance and density of states for the B-doped (site #2) 11-aGNR open system, and band structure of the periodic system, where no spin-dependence is observed. Energies are relative to the Fermi energy of the leads. The arrow shows the approximate energy range of the charge density calculation in b. (b) Spin down charge density (isovalue = 0.001 e·Bohr^{-3}) for the energy range -0.62 eV to -0.37 eV, showing the localization of the states at this energy range. The spin up charge density is identical and not shown. H atoms are shown in light color (yellow), C atoms are shown in gray, and B atoms are shown as lighter gray (green) circles.

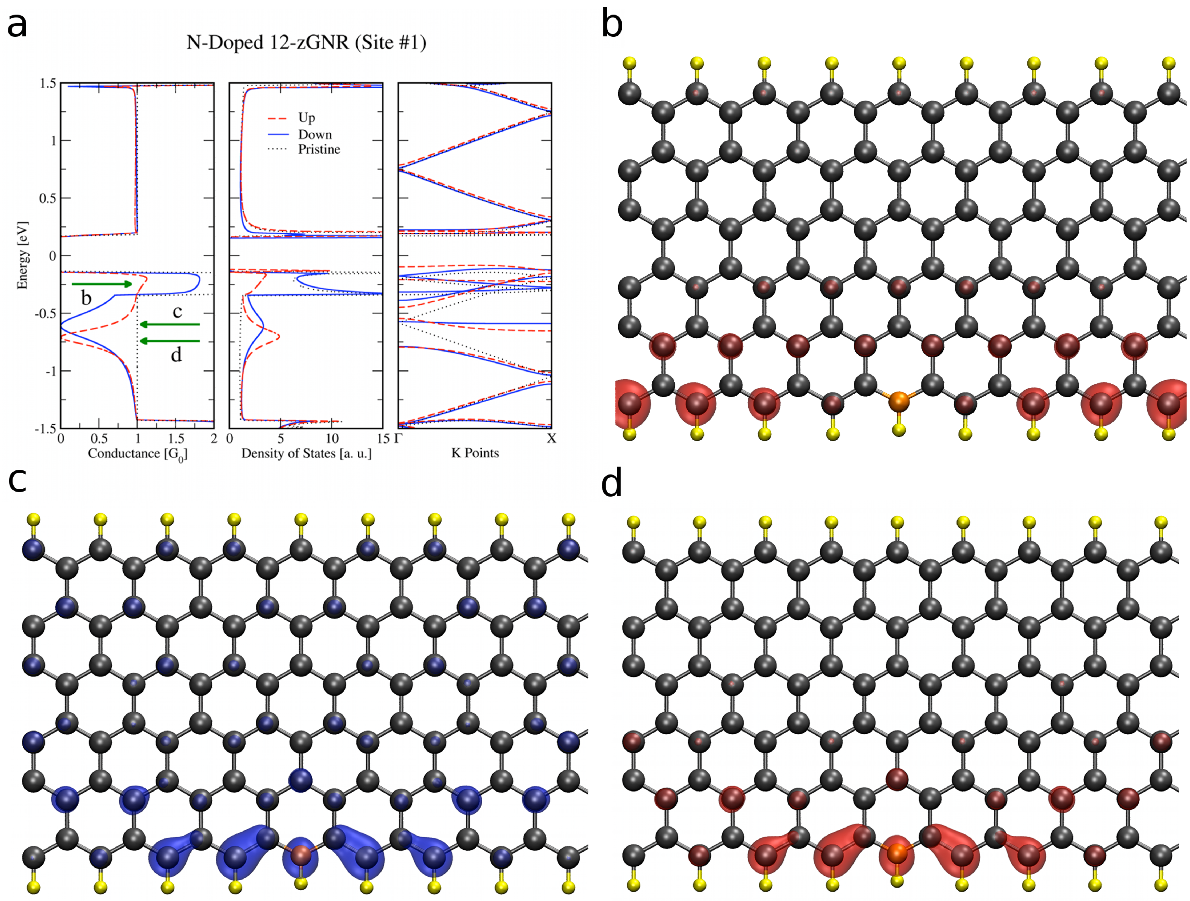

Figure 5: ***(color online)*** (a) Conductance and density of states for the N-doped (site #1) 12-zGNR open system, and band structure of the periodic system. Energies are relative to the Fermi energy of the leads. Arrows mark the approximate energy ranges where conductance dips or spin-dependence is observed, and where charge density calculations were performed. (b) Spin up charge density for the energy range -0.37 eV to -0.21 eV. (c) Spin down charge density for the energy range -0.86 eV to -0.65 eV. (d) Spin up charge density for the energy range -0.79 eV to -0.50 eV. All isosurfaces were drawn at density=0.008 e·Bohr^{-3}, and H atoms are shown in light color (yellow), C atoms are shown in gray, and N atoms are shown as lighter gray (orange) circles.

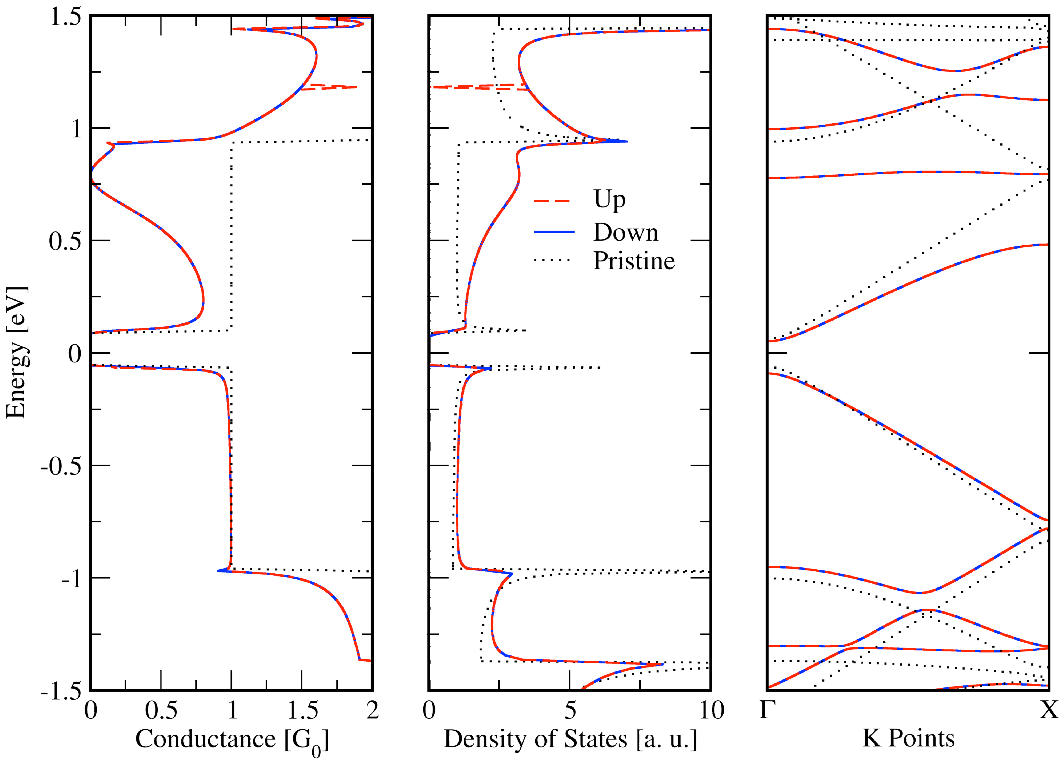

Figure 6: **(color online)** Conductance and density of states for the N-doped (site #1) 11-aGNR open system, and band structurecof the periodic system showing spin-degenerate behavior, and a dip of conductance at 0.8 eV caused by the nitrogen-induced localized state. Energies are relative to the Fermi energy of the leads.

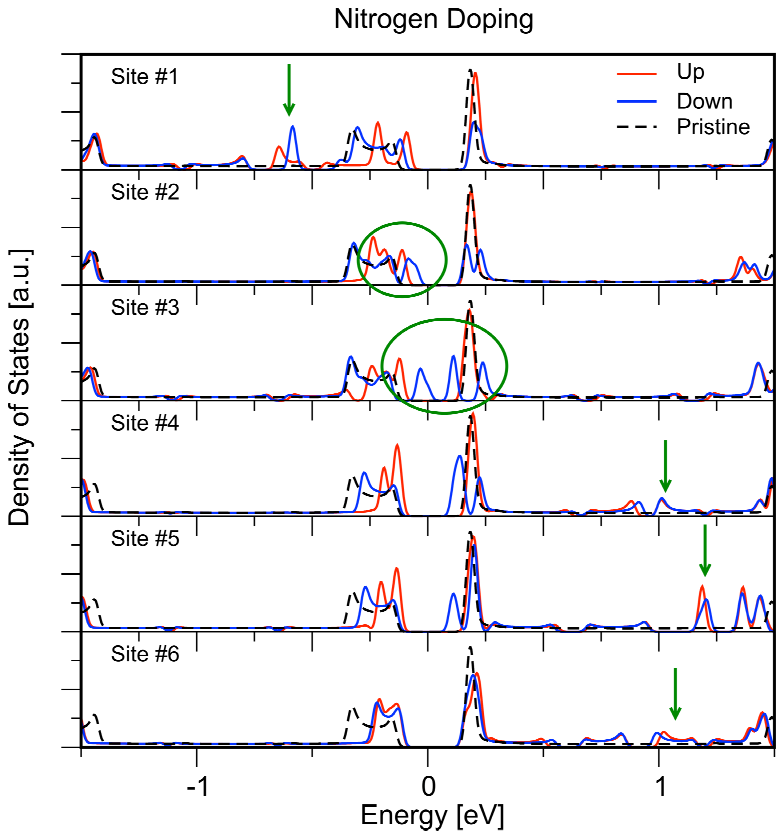

Figure 7: (color online) Density of states for nitrogen-doped zigzag graphene nanoribbons, for doping atom position ranging from the center (site #6, bottom) to the edge of the nanoribbon (site #1, top). As the atom is moved closer to the edge, electrostatic interactions between the localized states and the carbon edge state cause shifts in the energy of the localized states (arrows, sites #4-6), splitting of the edge states (circled areas, sites #2-3) and finally the shift of the localized state towards the valence bands (arrow, site #1). Energies are relative to the pristine nanoribbon's Fermi energy.

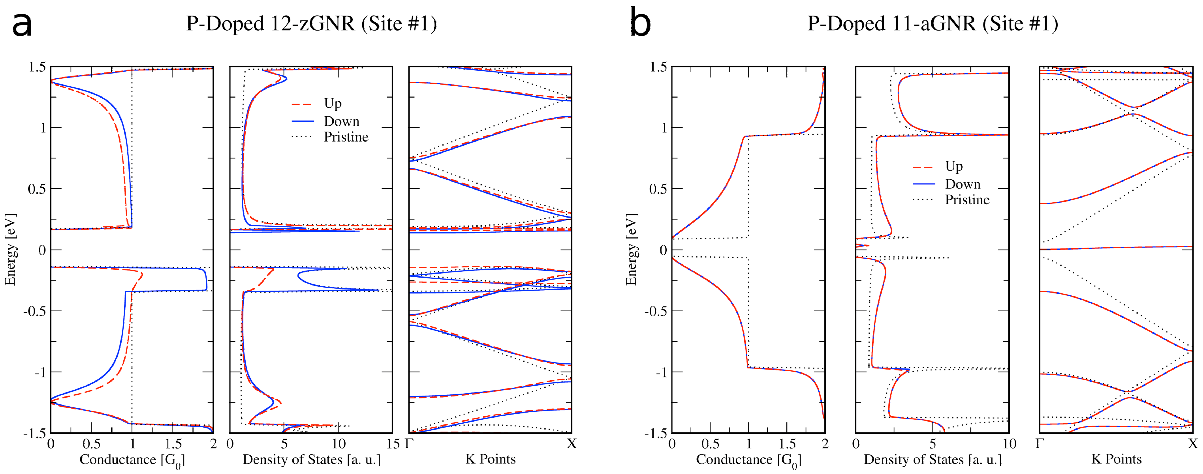

Figure 8: (color online) Conductance and density of states of an open system, and band structure of a periodic system, of the (a) P-doped (site #1) 12-zGNR structure, and (b) P-doped (site #1) 11-aGNR structure. The 12-zGNR structure exhibits both a donor and an acceptor state, whereas the 11-aGNR structure exhibits a wide drop in conductance centered on the Fermi energy. Energies are relative to the Fermi energy of the leads.

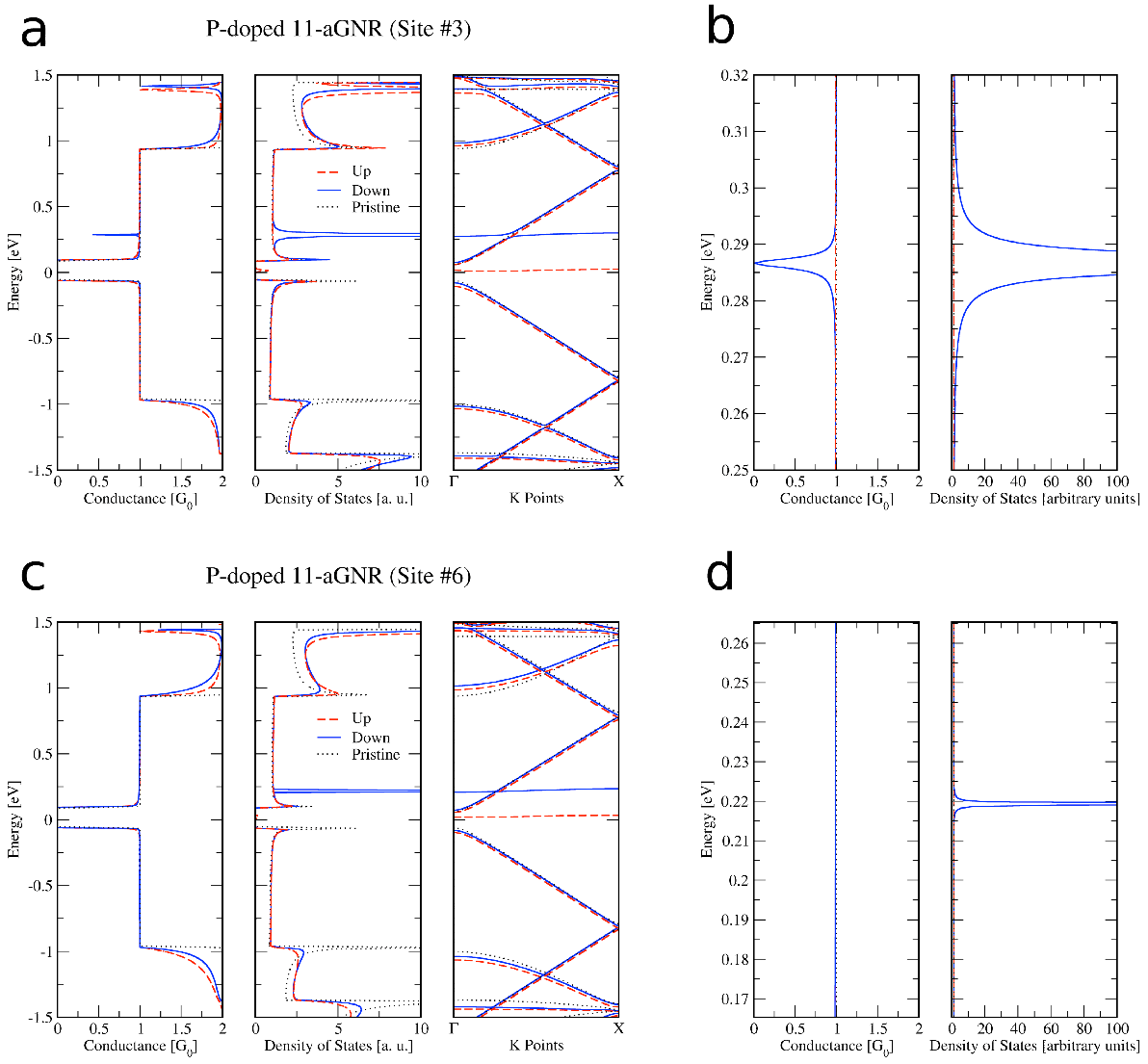

Figure 9: (color online) Conductance and density of states of an open system, and band structure of a periodic system, for P-doped (a) site #3, and (c) site #6 structures of 11-aGNR. Spin-dependent behavior appears in both structures as a large spike in spin down states just above the Fermi energy, accompanied by a flat band. (b) and (d) show a zoomed in view of the conductance and density of states for site #3 and site #6 around the energy range of the spike in spin down states. Energies are relative to the Fermi energy of the leads. The spike in spin down states is shown to cause a drop to zero conductance for the site #3 structure while having no impact on the conductance in the site #6 structure.

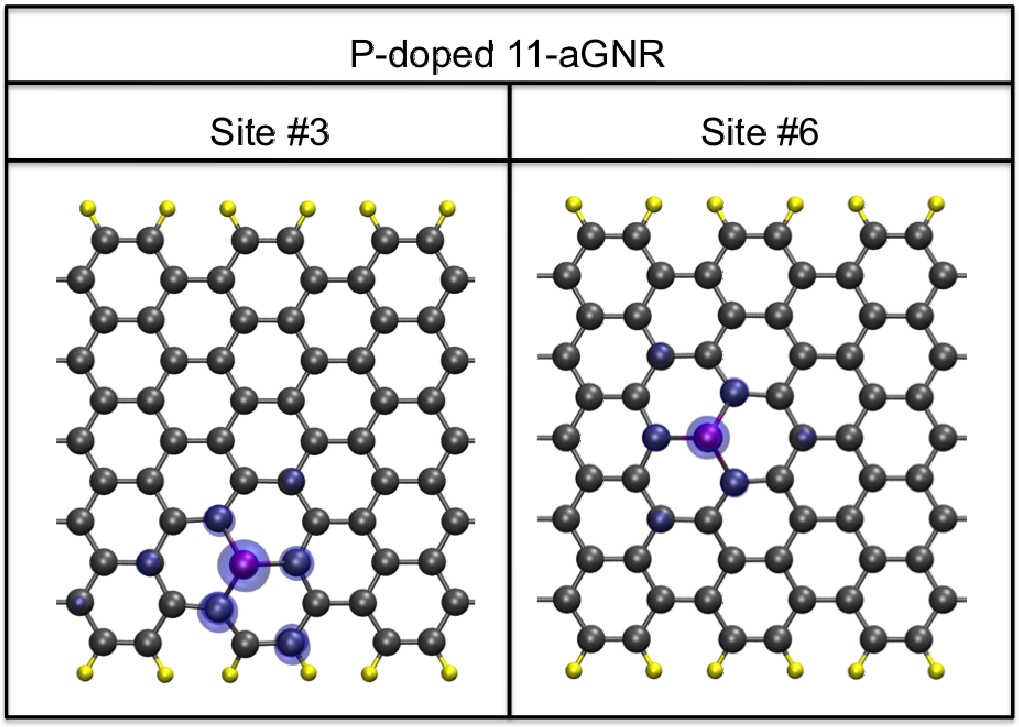

Figure 10: **(color online)** Spin down charge density in a P-doped 11-aGNR (site #3) and a P-doped 11-aGNR (site #6) for the energy range in which the spike in spin down states occurs (0.21 eV to 0.23 eV for site #3 and 0.011 eV to 0.18 eV for site #6), with energies relative to the Fermi energy for the leads. H atoms are shown in light grey (yellow), C atoms are shown in gray, and P atoms are shown as larger dark grey circles.